

Application of Gauss-Newton method in magnetic dipole model

Junchen Gao(高骏琛), Chaobo Liu(刘超波), Jinjing Zhang(张津菁), Yu Duan(段宇), Hao-Ran Yang(杨浩冉), and Daqiang Gao(高大强)

Citation: Chin. Phys. B, 2025, 34 (**10**): 100701. DOI: 10.1088/1674-1056/addcd1
http://cpb.iphy.ac.cn; http://iopscience.iop.org/cpb

What follows is a list of articles you may be interested in

Spin-based magnetic detection of optically trapped single cell in microfluidic channel

Jun Yin(殷俊), Sanyou Chen(陈三友), Yihao Yan(燕一皓), Mengqi Wang(王孟祺), Ya Wang(王亚), Yiheng Lin(林毅恒), Qi Zhang(张琪), and Fazhan Shi(石发展)

Chin. Phys. B, 2025, 34 (**7**): 070704. DOI: 10.1088/1674-1056/adde38

Blind parameter estimation of pseudo-random binary code-linear frequency modulation signal based on Duffing oscillator at low SNR

Ke Wang(王珂), Xiaopeng Yan(闫晓鹏), Ze Li(李泽), Xinhong Hao(郝新红), and Honghai Yu(于洪海)

Chin. Phys. B, 2021, 30 (**5**): 050708. DOI: 10.1088/1674-1056/abd75f

A high performance fast-Fourier-transform spectrum analyzer for measuring spin noise spectrums

Yu Tong(仝煜), Lin Wang(王淋), Wen-Zhe Zhang(张闻哲), Ming-Dong Zhu(朱明东), Xi Qin(秦熙), Min Jiang(江敏), Xing Rong(荣星), Jiangfeng Du(杜江峰)

Chin. Phys. B, 2020, 29 (**9**): 090704. DOI: 10.1088/1674-1056/ab9c04

Experimental research on spectrum and imaging of continuous-wave terahertz radiation based on interferometry

Tie-Lin Lu(卢铁林), Hui Yuan(袁 慧), Ling-Qin Kong(孔令琴), Yue-Jin Zhao(赵跃进), Liang-Liang Zhang(张亮亮), Cun-Lin Zhang(张存林)

Chin. Phys. B, 2016, 25 (**8**): 080702. DOI: 10.1088/1674-1056/25/8/080702

Thermal efficiency of the principal greenhouse gases

A. Y. Galashev, O. R. Rakhmanova

Chin. Phys. B, 2015, 24 (**1**): 010701. DOI: 10.1088/1674-1056/24/1/010701

Application of Gauss–Newton method in magnetic dipole model

Junchen Gao(高骏琛)[1], Chaobo Liu(刘超波)[2], Jinjing Zhang(张津菁)[1], Yu Duan(段宇)[1], Hao-Ran Yang(杨浩冉)[1], and Daqiang Gao(高大强)[1,†]

[1] *College of Physical Science and Technology, Key Laboratory of Magnetism and Magnetic Materials, Ministry of Education, Lanzhou University, Lanzhou* 730000, *China*

[2] *Beijing Institute of Spacecraft Environment Engineering, Beijing* 100000, *China*

(Received 24 March 2025; revised manuscript received 19 May 2025; accepted manuscript online 26 May 2025)

With the increasing accuracy requirements of satellite magnetic detection missions, reducing low-frequency noise has become a key focus of satellite magnetic cleanliness technology. Traditional satellite magnetic simulation methods have matured in static magnetic dipole simulations, but there is still significant room for optimization in the simulation and computation of low-frequency magnetic dipole models. This study employs the Gauss–Newton method and Fourier transform techniques for modeling and simulating low-frequency magnetic dipoles. Compared to the traditional particle swarm optimization (PSO) algorithm, this method achieves significant improvements, with errors reaching the order of 10^{-13}% under noise-free conditions and maintaining an error level of less than 0.5% under 10% noise. Additionally, the use of Fourier transform and the Gauss–Newton method enables high-precision magnetic field frequency identification and rapid computation of the dipole position and magnetic moment, greatly enhancing the computational efficiency and accuracy of the model.

Keywords: magnetic dipole model, Gauss–Newton method, Fourier transform, inversion accuracy

PACS: 07.55.Ge, 02.30.Zz, 41.20.Gz, 02.60.Pn

DOI: 10.1088/1674-1056/addcd1 **CSTR:** 32038.14.CPB.addcd1

1. Introduction

The magnetic design of satellites is a fundamental aspect of space engineering, essential for mitigating magnetic interference and ensuring optimal satellite performance.[1,2] Magnetic interference primarily arises from internal electromagnetic components and external sources, including Earth's geomagnetic field and solar activity.[3,4] Accurate modeling and optimization of the magnetic field are crucial not only for improving attitude control precision but also for enhancing the stability and accuracy of onboard instrumentation.[5,6]

Among various modeling approaches, the magnetic dipole model has gained prominence due to its theoretical simplicity and computational efficiency.[7] By decomposing complex magnetic fields into multiple dipole components, it effectively represents both internal interference sources and external environmental fields. To refine magnetic interference localization, shielding optimization, and compensation design, various optimization algorithms have been integrated into dipole modeling.[8,9] One such a technique, particle swarm optimization (PSO), is widely employed due to its flexibility and effectiveness in solving nonlinear optimization problems with minimal reliance on gradient information.[9,10] However, PSO has notable drawbacks, including limited convergence accuracy and high sensitivity to initial parameter selection, which can lead to suboptimal solutions.[11–13]

In contrast, the Gauss–Newton (GN) method, a gradient-based optimization technique, employs a second-order approximation of the objective function to achieve rapid and precise iterative convergence. This method demonstrates superior accuracy and efficiency, particularly when reasonable initial values are provided and the problem exhibits locally linear behavior.[14,15] Unlike PSO, the GN method is highly effective in scenarios where gradient information is readily available, making it particularly suitable for high-precision magnetic field modeling and parameter inversion.[16]

Given the relatively small number of parameters in satellite magnetic design, the GN method often achieves higher accuracy than global optimization methods. In the context of low-frequency magnetic dipole models (3 Hz–3000 Hz), it accurately reconstructs dipole magnetic moments while maintaining robustness against measurement noise and interference. Even under varying levels of error, the GN method consistently recovers the dipole parameters with high reliability. Despite advances in magnetic dipole modeling, existing approaches remain inadequate for low-frequency simulations, and the multi-solution nature of the dipole model frequently leads to ambiguities when using PSO in practical applications. To address these challenges, this study employs the GN method combined with gradient descent techniques to optimize the inversion of magnetic dipole models. To improve the classical GN method and make it more suitable for low-frequency magnetic dipole inversion, this study introduces

[†]Corresponding author. E-mail: gaodqxz@sina.com

© 2025 Chinese Physical Society and IOP Publishing Ltd. All rights, including for text and data mining, AI training, and similar technologies, are reserved.

several novel strategies. First, a Fourier-based preprocessing step is employed to isolate the dominant frequency components of the magnetic field signal, which reduces the inversion parameter space from a three-dimensional (position, moment, frequency) to a two-dimensional (position and moment) problem. This significantly enhances the inversion speed and robustness. Second, realistic spatial constraints based on the physical structure of the spacecraft are integrated into the optimization framework to improve convergence reliability and solution uniqueness. Third, L2 regularization is introduced into the cost function to penalize large parameter estimates and avoid overfitting, especially under noisy conditions. Finally, to address sensitivity to initial values, the GN method is initialized using multiple heuristically chosen magnetic moments based on typical system scales. These improvements collectively strengthen the GN method's stability and performance in low-frequency magnetic field inversion.

2. Theoretical model

2.1. Magnetic dipole model

The modeling process begins with forward modeling to simulate the magnetic field distribution generated by magnetic dipoles. Assuming each magnetic dipole has a fixed magnetic moment and position , the magnetic field at a specific point is given by

$$B_{\mathrm{t}}(\boldsymbol{R}) = \frac{\mu_0}{4\pi}\left[\frac{3(\boldsymbol{R}-\boldsymbol{R}_{\mathrm{t}})(\boldsymbol{R}-\boldsymbol{R}_{\mathrm{t}})\boldsymbol{M}_{\mathrm{t}}}{|\boldsymbol{R}-\boldsymbol{R}_{\mathrm{t}}|^5} - \frac{\boldsymbol{M}_{\mathrm{t}}}{|\boldsymbol{R}-\boldsymbol{R}_{\mathrm{t}}|^3}\right], \quad (1)$$

where $\boldsymbol{M}_{\mathrm{t}}$ is the magnetic moment, $\boldsymbol{R}_{\mathrm{t}}$ is the position of the dipole, and $\boldsymbol{R}$ is the position of the test point.

In Fig. 1(a), 12 test points were distributed on two circular planes to improve spatial diversity and reduce geometric bias. Specifically, one circle was placed at $z = 0.1$ m with a radius of 1.4 m, and the other at $z = -0.1$ m with a radius of 2.4 m.[17] Each circle contained six test points arranged counterclockwise at 60° intervals starting from the positive x-axis direction. This dual-plane configuration ensures better vertical coverage and enhances inversion accuracy compared to a single-ring layout.

To mitigate the dependency on initial parameters, especially in the GN method, two strategies are adopted in our model. First, spatial constraints are imposed on the dipole position parameters based on actual experimental setup, where dipole positions can be measured with millimeter-level precision. This restricts the initial position estimates to a narrow and physically valid region. Second, we apply a Fourier transform to the measured magnetic field data, enabling clear identification of dominant frequency components. The inversion algorithm is then guided by frequency-domain priors, regularized using L2 norms to prevent overfitting and stabilize convergence. Since position and frequency are relatively constrained, the primary inversion uncertainty lies in estimating magnetic moments. Therefore, we adopt an ensemble initialization strategy using multiple sets of magnetic moments with gradually increasing magnitudes and uniformly sampled directions, effectively enhancing the robustness and success rate of the inversion.

The magnetic field at each test point is denoted as $\boldsymbol{B}_{\mathrm{t}}$. To simulate real-world measurement conditions, 5% random noise $\boldsymbol{n}$ is added to the magnetic field data:

$$\boldsymbol{B}'_{\mathrm{t}} = \boldsymbol{B}_{\mathrm{t}} + \boldsymbol{n}\boldsymbol{B}_{\mathrm{t}}, \quad (2)$$

where $\boldsymbol{n}$ is the random noise with an amplitude equal to 5% of the magnetic field strength. The noisy magnetic field data $\boldsymbol{B}'_{\mathrm{t}}$ serves as input for the inversion process, reflecting the impact of measurement uncertainties on the model's accuracy. [18,19]

2.2. Gauss–Newton method

To enhance the effectiveness of the GN method in low-frequency magnetic dipole inversion, several targeted improvements were incorporated in this study. We introduced a Fourier transform-based preprocessing step to extract the dominant frequency components from the measured magnetic field. This reduced the inversion parameter space from three dimensions (magnetic moment, position, and frequency) to two (magnetic moment and position), significantly enhancing both convergence speed and inversion precision. Physical spatial constraints were added to the inversion process. In practical satellite systems, the positions of magnetic dipoles (*e.g.*, components or cables) are physically fixed and measurable to millimeter-level accuracy. By constraining the dipole locations within realistic boundaries, the solution space is narrowed, mitigating issues caused by overlapping fields and enhancing uniqueness. Then we adopted an L2 regularization strategy to improve stability under noise. The loss function was redefined to incorporate a weighted sum of the squared relative residuals and a penalty term for the parameter norm:

$$\min_{p}\left(\sum_{i=1}^{n}\left[\frac{y_i - f(x_i,p)}{y_i}\right]^2 + \lambda\,\|p\|^2\right), \quad (3)$$

where y_i is the noisy observed field, $f(x_i,p)$ is the predicted field, and λ is the regularization coefficient. This formulation allows the algorithm to penalize large deviations while avoiding overfitting to noisy data.

The residual vector $\boldsymbol{r}(p)$ is defined as follows:

$$\boldsymbol{r}(p) = [y_1 - f(x_1,p), y_2 - f(x_2,p), \ldots, y_n - f(x_n,p)]^{\mathrm{T}}. \quad (4)$$

The Jacobian matrix $\boldsymbol{J}$ represents the partial derivatives of the model output with respect to the parameters

$$J_{ij} = \frac{\partial f(x_i, p)}{\partial p_j}. \tag{5}$$

The parameter updates are performed iteratively using the following formula:

$$p_{k+1} = p_k + \left(\boldsymbol{J}^{\mathrm{T}}\boldsymbol{J}\right)^{-1}\boldsymbol{J}^{\mathrm{T}}\boldsymbol{r}(p_k). \tag{6}$$

This study also compares the GN method with the PSO algorithm. While PSO is a classical global search algorithm, it exhibits an error margin of approximately 5%. In contrast, the GN method demonstrates superior accuracy, particularly for low-dimensional parameter matrices. For magnetic dipole models with only two unknown variables (magnetic moment and position), the GN method can achieve nearly perfect inversion of the simulated magnetic field.

To address the GN method's sensitivity to initial parameter values, we design a heuristic initialization strategy. A range of linearly spaced initial magnetic moments is generated, and multiple inversion attempts are executed in parallel. This significantly increases the likelihood of converging to the global optimum, especially in complex or noisy scenarios with multiple local minima.

Together, these improvements make the GN method highly effective for practical low-frequency magnetic dipole modeling tasks. Compared to classical global optimization methods like PSO in Figs. 1(b)–1(e), the enhanced GN approach offers faster convergence, requires fewer measurement points, and achieves superior inversion accuracy. Its strong resistance to noise and efficient use of gradient information make it a promising tool for applications such as magnetic field imaging, geophysical surveys, and complex magnetic source reconstruction.

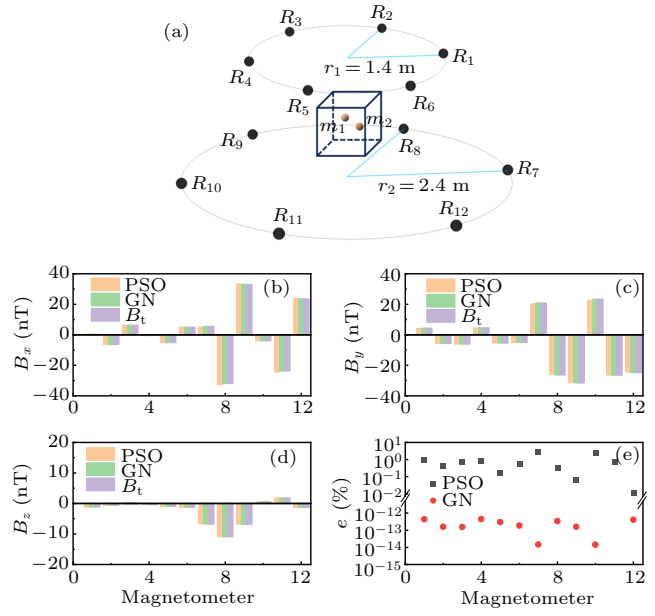


Fig. 1. (a) Schematic diagram of magnetic dipole test points. (b)–(d) Comparisons of inversion results between the PSO method and the GN method for B_x, B_y, and B_z components. (e) Inversion error results of the PSO and GN methods.

3. Experimental simulation verification

This section provides a comprehensive analysis of the results obtained from the magnetic dipole inversion study based on the Gauss–Newton (GN) method, with a focus on inversion performance under static conditions, low-frequency scenarios, and multi-dipole systems.[10,14,21]

3.1. Single magnetic dipole model

The analysis begins with the evaluation of the GN method's effectiveness in reconstructing magnetic field distributions for both single and double magnetic dipole models. In the case of a single dipole, as shown in Fig. 2(a), the simulated magnetic field ($\boldsymbol{B}_t$) and the inverted magnetic field ($\boldsymbol{B}_d$) exhibit a high degree of agreement, demonstrating the accuracy of the GN method in solving inversion problems. Furthermore, the residual error analysis in Fig. 2(a) shows minimal discrepancies, highlighting the algorithm's robustness in static conditions. The calculation error e of the single dipole model remains within 5%, which is lower than the predefined error threshold used when generating the simulated magnetic field data.

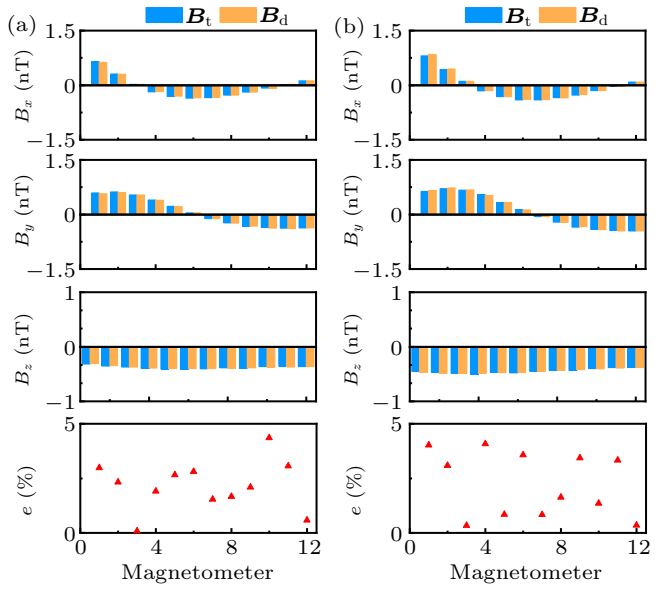


Fig. 2. (a) Comparisons of the x, y, and z components of the forward magnetic field $\boldsymbol{B}_t$ and the inverted magnetic field $\boldsymbol{B}_d$ for a single magnetic dipole, along with the error e diagram. (b) Comparisons of the x, y, and z components of the forward magnetic field $\boldsymbol{B}_t$ and the inverted magnetic field $\boldsymbol{B}_d$ for two magnetic dipoles, along with the error e diagram.

For two static magnetic dipoles, the GN method continues to exhibit strong inversion capabilities. Magnetic dipole inversion is inherently an ill-posed problem, as a given observed magnetic field distribution may correspond to multiple sets of dipole parameters. This non-uniqueness arises from the nonlinear superposition of magnetic fields and the complex interactions between dipoles. For example, when two or more dipoles are positioned closely together or their magnetic fields significantly overlap, multiple parameter solutions may emerge, leading to ambiguous inversion outcomes.

To address this issue, spatial constraints on dipole placement are introduced during the optimization process, ensuring solution uniqueness and mitigating the effects of overlapping magnetic fields. As shown in Fig. 2(b), the residual error distribution indicates that, compared to the single-dipole case, the double-dipole scenario exhibits slightly higher errors, with some values reaching approximately 4%. This increase is attributed to the added complexity of dipole interactions. However, the overall errors remain below 5%, confirming the reliability of the GN method in handling static multi-dipole systems.

3.2. Low-frequency magnetic dipole model

To further analyze the inversion process, a Fourier transform is applied to the dual magnetic dipole model. The resulting frequency domain distributions, presented in Figs. 3(a) and 3(b), reveal two distinct peaks corresponding to the superposition of magnetic fields generated by the two dipoles. The Fourier transform effectively decomposes these superimposed signals, isolating the frequency components of each dipole, which significantly enhances both the accuracy and stability of the inversion solution.

In the case of the multi-dipole model, as shown in Fig. 3(c), the frequency domain distribution exhibits multiple distinct peaks, highlighting the complex superposition characteristics of multi-dipole signals. Despite the increased signal complexity, the peaks remain well-defined, demonstrating the Fourier transform's capability to accurately decompose complex multi-source magnetic field signals. This ability is particularly valuable in distinguishing individual dipole contributions in environments where multiple sources coexist.

The Fourier transform provides several key advantages in the inversion of low-frequency magnetic dipole signals. First, it efficiently extracts the primary frequency components of the magnetic field, allowing for a clearer representation of the signal structure. Second, by transforming the problem into the frequency domain, it reduces the dimensionality of the parameter space, which in turn decreases computational complexity during the inversion process. This not only improves computational efficiency but also enhances the overall accuracy and stability of the inversion results.

By leveraging the Fourier transform in conjunction with the GN method, this study establishes a robust framework for low-frequency magnetic dipole inversion. The ability to isolate and analyze frequency components independently ensures that the inversion process remains resilient against noise and external interference. These advantages provide a solid theoretical foundation and technical assurance for the practical application of low-frequency magnetic dipole inversion in various fields, including geophysical exploration, magnetic field imaging, and complex parameter estimation.

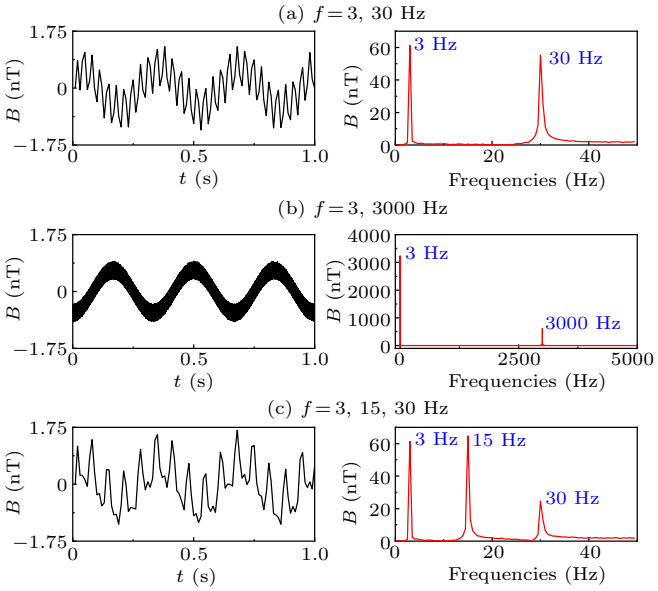


Fig. 3. (a) Schematic diagram illustrating the magnetic field variation over time at the point (0, 0, 2.4 m) for the 3-Hz and 30-Hz dipole models, along with their frequency–domain representation after Fourier transform. (b) Schematic diagram showing the magnetic field variation over time at the point (0, 0, 2.4 m) for the 3-Hz and 3000-Hz dipole models, accompanied by their frequency–domain representation after Fourier transform. (c) Schematic diagram presenting the magnetic field variation over time at the point (0, 0, 2.4 m) for the 3-Hz, 15-Hz, and 30-Hz dipole models, together with their frequency–domain representation after Fourier transform.

Under low-frequency conditions (3 Hz and 30 Hz), experimental results further validate the accuracy and robustness of the GN method in reconstructing magnetic fields. As shown in Fig. 4(a), the inverted magnetic field $\boldsymbol{B}_{\mathrm{d}}$ closely matches the simulated magnetic field $\boldsymbol{B}_{\mathrm{t}}$, indicating that the method effectively processes low-frequency signals. The error plots further confirm the method's reliability, with minimal deviations observed between $\boldsymbol{B}_{\mathrm{d}}$ and $\boldsymbol{B}_{\mathrm{t}}$, reinforcing its accuracy in low-frequency inversion tasks.

This capability has significant implications for practical applications, such as geophysical exploration and biomedical magnetic field modeling, where low-frequency magnetic signals play a crucial role. The GN method's consistent performance across these frequencies demonstrates its stability and adaptability in low-frequency scenarios. Unlike conventional global optimization methods, which often require extensive computational resources and struggle with local minima, the GN method leverages gradient-based optimization to refine solutions with high precision, ensuring reliable results even under varying conditions.

To assess the applicability of the GN method across a broader frequency spectrum, inversion results were also analyzed for higher frequencies, including up to 3000 Hz. As illustrated in Fig. 4(b), the simulated magnetic field $\boldsymbol{B}_{\mathrm{t}}$ and the inverted magnetic field $\boldsymbol{B}_{\mathrm{d}}$ remain in good agreement even at high frequencies, though a slight increase in residual errors is observed compared to low-frequency conditions. This increase can be attributed to the higher sensitivity of high-frequency signals to initial parameter settings, as well as the

accumulation of nonlinear effects during numerical computations. Nevertheless, the GN method maintains sufficient adaptability for high-frequency scenarios, making it a valuable tool for applications requiring detailed high-frequency magnetic field modeling, such as electromagnetic compatibility testing and high-resolution magnetic imaging.

To further enhance inversion accuracy at high frequencies, improving initial parameter estimation and introducing stricter constraint conditions could help mitigate sensitivity-related errors. Incorporating adaptive filtering techniques or hybrid optimization approaches may also improve the stability of high-frequency magnetic field inversions, ensuring more robust results in practical applications.

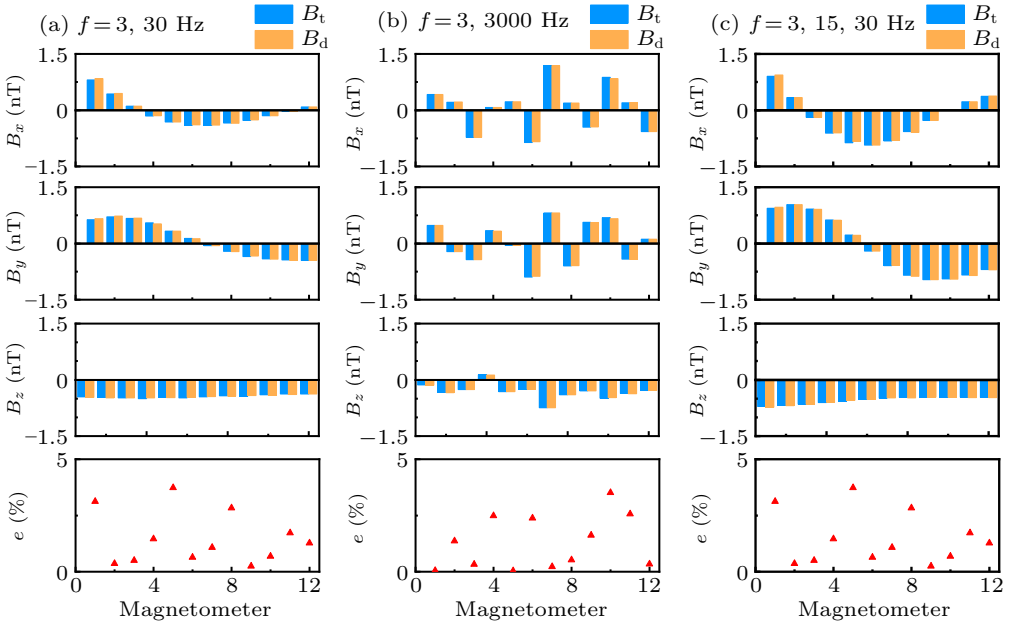


Fig. 4. (a) Comparisons of x, y, and z components of the forward magnetic field $\boldsymbol{B}_t$ and the inverted magnetic field $\boldsymbol{B}_d$ at 3 Hz and 30 Hz for the magnetic dipole, along with the error e diagram. (b) Comparisons of x, y, and z components of the forward magnetic field $\boldsymbol{B}_t$ and the inverted magnetic field $\boldsymbol{B}_d$ at 3 Hz and 3000 Hz for the magnetic dipole, along with the error e diagram. (c) Comparisons of x, y, and z components of the forward magnetic field $\boldsymbol{B}_t$ and the inverted magnetic field $\boldsymbol{B}_d$ at 3 Hz, 15 Hz, and 30 Hz for the magnetic dipole, along with the error e diagram.

3.3. Model noise resistance test

Beyond single and dual dipole systems, the study extends to multi-dipole configurations under low-frequency conditions. The inversion results for three magnetic dipoles at 3 Hz, 15 Hz, and 30 Hz further demonstrate the GN method's ability to handle complex inversion scenarios. As shown in Fig. 4(c), the inverted magnetic field $\boldsymbol{B}_d$ exhibits high fidelity to the simulated magnetic field $\boldsymbol{B}_t$, confirming the method's accuracy in resolving multiple dipole sources at different frequency ranges.

Error analysis reveals a stable error distribution across the multi-dipole system, with primary deviations influenced by the added noise in the simulated field $\boldsymbol{B}_t$. This finding highlights the GN method's robustness in addressing multi-source inversion problems, a crucial requirement for applications such as subsurface resource exploration and complex electromagnetic environment simulations.

Despite the increased computational complexity associated with multi-dipole systems, advancements in parallel computing and algorithmic optimization can effectively mitigate computational overhead. By leveraging modern high-performance computing techniques, the GN method remains an efficient and scalable approach for large-scale multi-dipole inversion, ensuring practical feasibility in real-world applications.

To evaluate the robustness of the GN method under noisy conditions, varying levels of noise were introduced into the inverted magnetic field $\boldsymbol{B}_d$. Even under low signal-to-noise ratio (SNR) conditions, the inversion results exhibit minimal deviations, successfully capturing the key characteristics of the original field distribution. The reconstructed magnetic moment closely aligns with the simulated magnetic moment, further validating the reliability of the inversion method.

In Figs. 5(a)–5(c), when different levels of noise ($n = 0\%$, 5%, 10%) were added to $\boldsymbol{B}_t$, the algorithm effectively filtered out interference while preserving the primary signal structure. This resilience can be attributed to the GN optimization process, which iteratively minimizes residual errors between observed and reconstructed magnetic fields, ensuring stability against noise-induced perturbations.

Statistical analysis of the GN model inversion results indicates that even when the noise ratio reaches 10%, the variance and bias of the reconstructed magnetic moments remain within 1%. This confirms the method's robustness in handling practical scenarios, where noise is often unavoidable due to sensor limitations, environmental disturbances, or measurement

errors. Consequently, the GN-based magnetic dipole model proves to be a reliable tool for applications requiring high-accuracy magnetic field reconstruction and magnetic moment estimation, even under challenging conditions with substantial noise interference.

The GN method's performance is further benchmarked against the PSO algorithm to assess its relative efficiency in solving magnetic dipole inversion problems. Compared to PSO, which relies on global search mechanisms, the GN optimization algorithm demonstrates significant advantages, particularly in cases where the number of inversion parameters is small. While global search algorithms typically require larger search spaces and greater computational resources to achieve global optimization, the GN method leverages its gradient-based fast convergence properties to precisely fit low-dimensional parameter matrices.

Experimental results show that the GN method requires fewer test points and less restrictive conditions while achieving high-precision inversion of magnetic moments and positions. In cases where the unknown variables include only the magnetic moments and positions of the dipoles, the GN method achieves inversion errors significantly lower than the approximately 5% error margin of the PSO algorithm, demonstrating exceptional accuracy and efficiency.

In addition to its optimization efficiency, the Fourier transform plays a crucial role in enhancing inversion performance by effectively decomposing complex magnetic field signals. The Fourier transform enables the clear separation of superimposed signals in the frequency domain, significantly improving inversion accuracy and stability. In multi-source magnetic dipole scenarios, frequency domain analysis reveals multiple distinct peaks corresponding to different dipoles, further validating the Fourier transform's capability in handling complex superimposed signals.

This characteristic proves advantageous in processing multi-source magnetic field data, effectively reducing computational complexity while substantially improving inversion accuracy. By integrating Fourier transform techniques with the GN method, this study establishes a highly efficient framework for magnetic dipole inversion, paving the way for further advancements in low-frequency and high-precision magnetic modeling applications.

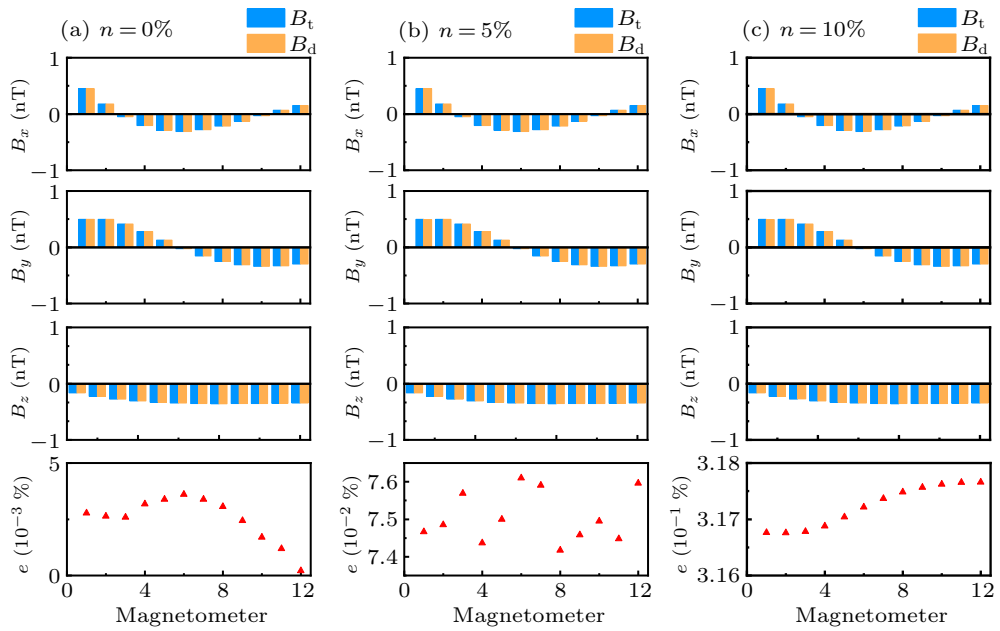


Fig. 5. Panels (a), (b), and (c) respectively show the comparison results between the inverted magnetic field $\boldsymbol{B}_{\rm d}$ and the error-free simulated magnetic field $\boldsymbol{B}_{\rm t}$ under the conditions of error-free $\boldsymbol{B}_{\rm t}$, $\boldsymbol{B}_{\rm t}$ with 5% noise ($n = 5\%$), and $\boldsymbol{B}_{\rm t}$ with 10% noise ($n = 10\%$).

4. Conclusion and perspectives

The inversion approach combining the GN method and Fourier transform provides a reliable and efficient solution for low-frequency magnetic dipole modeling. This framework offers a theoretical foundation and technical support for parameter estimation and stable inversion of low-frequency magnetic field signals in practical applications. Even in the presence of noise and complex conditions, it ensures the accuracy and stability of results.[6,17,21] Particularly when the number of inversion parameters is small, the GN method exhibits significantly greater efficiency and advantages over global search algorithms, providing a valuable reference for future inversion modeling of low-dimensional complex magnetic fields.

Acknowledgement

Project supported by the National Key Research and Development Program of China (Grant No. 2023YFC2206003).

References

[1] Langel R A and Hinze W J 1998 *The Magnetic Field of the Earth's Lithosphere: The Satellite Perspective* (Cambridge: Cambridge University Press) pp. 1–393

[2] Friis-Christensen E and Lühr H, Hulot G 2006 *Earth Planets Space* **58** 351

[3] Acuna M H 2002 *Rev. Sci. Instrum.* **73** 3717

[4] Tauxe L 2010 *Essentials of Paleomagnetism* (Berkeley: University of California Press) pp. 1–489

[5] Constable C G and Parker R L 1988 *J. Geophys. Res. Solid Earth* **93** 11569

[6] Love J J and Constable C G 2003 *Geophys. J. Int.* **152** 515

[7] Blakely R J 1996 *Potential Theory in Gravity and Magnetic Applications* (Cambridge: Cambridge University Press) pp. 1–356

[8] Kennedy J and Eberhart R 1995 *Proc. Int. Conf. Neural Networks*, November 27–December 1, 1995, Perth, Australia, pp. 1942–1945

[9] Nabighian M N, Grauch V J S, Hansen R O, LaFehr T R, Li Y, Peirce J W and Ruder M E, *et al.* 2005 *Geophysics* **70** 33

[10] Mehlem K 1978 *Spacecraft Electromagnetic Compatibility* **165** 165

[11] Mehlem K 1978 *IEEE Trans. Magn.* **14** 1064

[12] Pudney M A, Carr C M, Schwartz S J and Howarth S I 2013 *Geosci. Instrum. Method. Data Syst.* **2** 249

[13] Shi Y amd Eberhart R C 1999 *Proc. Congr. Evol. Comput.*, July 6–9, 1999, Washington DC, USA, pp. 1945–1950

[14] Carrubba E, Junge A, Marliani F and Monorchio A 2012 *Proc. ESA Workshop on Aerospace EMC*, May 21–23, 2012, Florence, Italy, pp. 1–6

[15] Mehlem K, Wiegand A and Weickert S 2012 *Proc. ESA Workshop on Aerospace EMC*, May 21–23, 2012, Florence, Italy, pp. 1–6

[16] Love J J and Rigler E J 2014 *Geophys. J. Int.* **199** 407

[17] Ovchinnikov M Y, Penkov V I, Roldugin D S and Pichuzhkina A V 2018 *Acta Astronaut.* **144** 171

[18] Srivastava R, Sah R, Das K 2021 arXiv: 2107.09257 [physics.geo-ph]

[19] Torbert R B, Dors I, Argall M R, Genestreti K J, Burch J L, Farrugia C J, Strangeway R J, *et al.* 2020 *Geophys. Res. Lett.* **47** e2019GL085542

[20] Dennis J E Jr, Schnabel R B 1996 *Numerical Methods for Unconstrained Optimization and Nonlinear Equations* (Philadelphia: SIAM) pp. 1–258

[21] Wright S J 2006 *Numerical Optimization* (New York: Springer) pp. 135–163